nature physics

ARTICLES

PUBLISHED ONLINE: 19 JANUARY 2014 | DOI: 10.1038/NPHYS2855

Liposome adhesion generates traction stress

Michael P. Murrell[1,2,3,4]*, Raphaël Voituriez[5], Jean-François Joanny[2,3,4], Pierre Nassoy[2,3,4,6†], Cécile Sykes[2,3,4†] and Margaret L. Gardel[1,7†]

Mechanical forces generated by cells modulate global shape changes required for essential life processes, such as polarization, division and spreading. Although the contribution of the cytoskeleton to cellular force generation is widely recognized, the role of the membrane is considered to be restricted to passively transmitting forces. Therefore, the mechanisms by which the membrane can directly contribute to cell tension are overlooked and poorly understood. To address this, we directly measure the stresses generated during liposome adhesion. We find that liposome spreading generates large traction stresses on compliant substrates. These stresses can be understood as the equilibration of internal, hydrostatic pressures generated by the enhanced membrane tension built up during adhesion. These results underscore the role of membranes in the generation of mechanical stresses on cellular length scales and that the modulation of hydrostatic pressure due to membrane tension and adhesion can be channelled to perform mechanical work on the environment.

The regulation of cell tension at the outer cell membrane is essential to a wide variety of morphogenetic processes such as division[1,2] migration[3] and spreading[4]. For instance, during cell adhesion and spreading, cells generate strong traction forces on the extracellular matrix (ECM) and a mechanical feedback between traction forces and ECM compliance is thought to influence cytoskeletal organization, cell spreading and migration[5]. Cellular force generation could arise from regulation of the cortical cytoskeleton (cortical tension) or from regulation of tension within the plasma membrane itself (membrane tension). The role of cortical tension in cellular force generation has been well established[6], and it is widely accepted that a membrane transmits forces[3,7]. However, the mechanisms by which pure membrane tension could contribute to forces generated by adherent cells are less understood, and were largely neglected because of the prevalence of the cytoskeleton as an active force generator. The central question addressed here is whether, beyond being a force transducer, a plasma membrane may also itself serve as a force generator.

In this study, we use cell-sized liposomes as a simple model system to probe the extent to which liposome adhesion facilitates changes in membrane tension balanced by mechanical stress on the substrate. Liposome spreading has been studied extensively on rigid surfaces, contributing to our understanding of the relationship between adhesion and membrane tension[8–10], and lipid phase behaviour[11,12], and more recently as a tool to probe the mechanical properties of a model cytoskeleton[13]. We study liposome spreading on deformable substrata. Surprisingly, our results show that adhesion of bare liposomes generates large stresses on compliant substrates. These stresses qualitatively alter the dynamics of liposome spreading on soft matrices, as they cause contraction of the contact area. We find that the measured traction stresses are consistent with the elevated hydrostatic pressures within the liposomes, and propose that the observed contraction of the substrate results from a minimization of the total energy that is the sum of adhesion and elastic contributions. As a secondary effect, this adhesion-induced contraction of the substrate often induces circular, phase-separated membrane domains at the contact line. Thus, our study illustrates the potential role of membrane adhesion not only in regulating tension and hydrostatic pressure but also in participating effectively in the generation of forces and their transmission to the ECM.

Results

Liposomes contract their contact area after initial spreading on soft substrates. Liposome spreading on glass substrates has been studied extensively[14–16] and follows four phases: approach of the liposome from the bulk solution to the surface of the substrate (P0), initial contact between the liposome and substrate (P1), formation of a flat interface between the liposome and substrate (P2/P3), and liposome rupture through the formation of a pore next to the contact line (P4; Fig. 1a,b). The first stage of spreading (P2) is fast, as the excess membrane adheres to the surface with little resistance, as has been observed previously[17]. P3 is slow, as the excess membrane is exhausted and increased spread area is limited by membrane tension increase[18]. Membrane tension increases to the point of lysis tension and the liposome eventually ruptures[19]. As lysis tension is $\sim$1 mN m^{-1}, considerable changes in membrane tension occur during liposome adhesion. However, the role of forces in liposome spreading has not been studied. Whereas the presence of hyaluronan cushions underneath a spreading liposome was shown to slow down the process[17], the magnitude of stresses that are transmitted to the substrate during spreading has not been measured. Moreover, the consequences of increased substrate compliance on liposome spreading have not been explored.

To study these questions, the adhesion and spreading of liposomes onto polyacrylamide (PAA) gels of variable elastic modulus (E) was monitored by imaging fluorescent lipids with confocal microscopy. Adhesion is mediated predominantly by the negative charges in the liposome, and the cationic poly-L-lysine chemically coupled to the surface of the PAA gel (Supplementary Fig. 1).

After initial contact with both stiff ($E = 165$ kPa) and soft ($E = 1.3$ kPa) gels coupled with 10 mg ml^{-1} poly-L-lysine, electroformed liposomes adhere and spread, gaining 90% of their

[1]Institute for Biophysical Dynamics, James Franck Institute, University of Chicago, Chicago, Illinois 60637, USA, [2]Institut Curie, Centre de Recherche, Laboratoire Physico-Chimie, UMR168, Paris F-75248, France, [3]Centre National de la Recherche Scientifique, UMR168, Paris F-75248, France, [4]Université Paris 6, Paris F-75248, France, [5]Laboratoire Jean Perrin, CNRS FRE 3231, and Laboratoire de Physique Théorique de la Matière Condensée, CNRS UMR 7600, Université Pierre et Marie Curie, 4 place Jussieu, Paris F-75005, France, [6]Institut d'Optique, LP2N, UMR 5298, Talence F-33405, France, [7]The Department of Physics, University of Chicago, Chicago, Illinois 60637, USA. †These authors contributed equally to this work. *e-mail: mmurrell2@wisc.edu

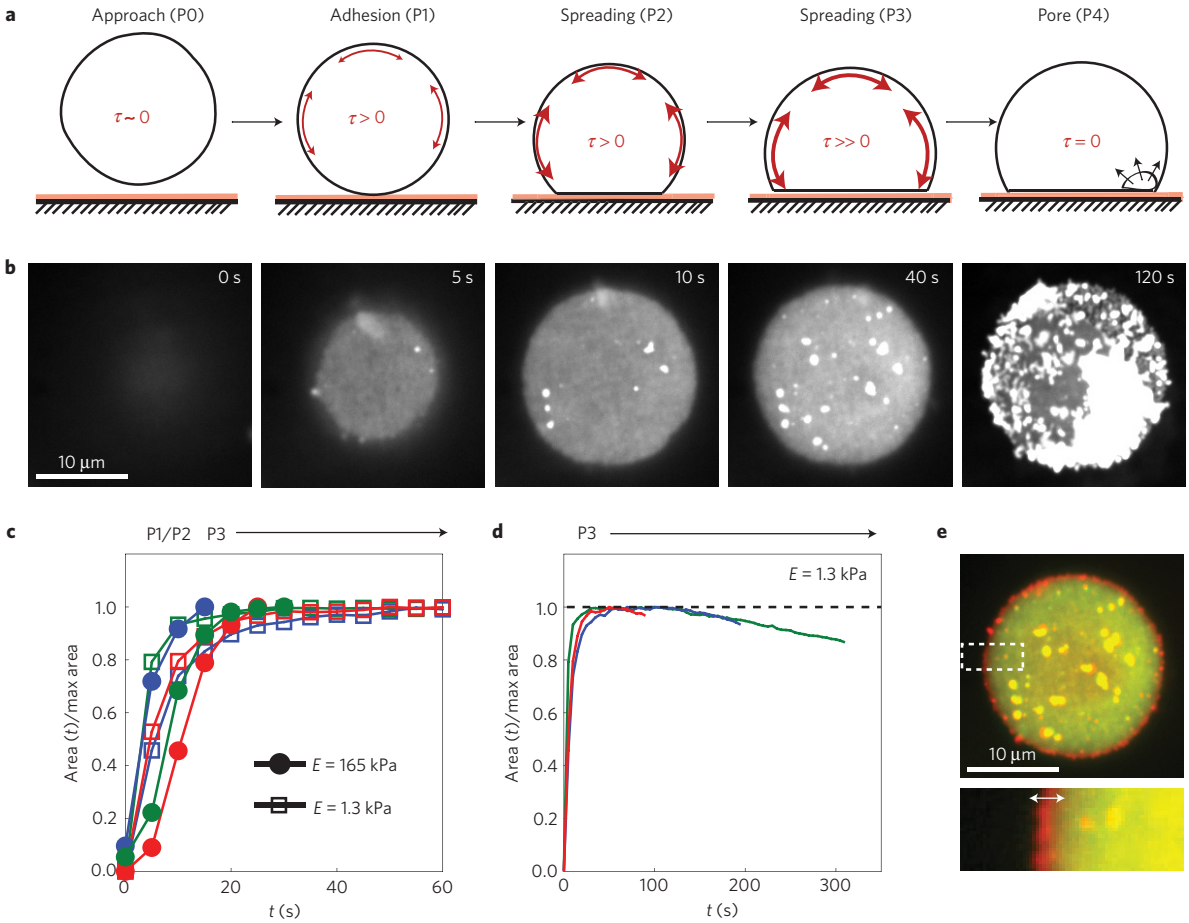

Figure 1 | The dynamics of liposome spreading depends on substrate stiffness. a, Diagram of liposome approach (P0), adhesion (P1) and spreading (P2/P3) on adhesive and stiff substrates that raises their membrane tension (τ, red arrows) and induces their rupture (P4). The width of the arrows reflects the magnitude of the tension. **b**, Liposome visualized by fluorescently labelled lipid (TR-DHPE) at the contact zone during the dynamics of spreading outlined in **a**. **c**, Normalized spread area over time for liposomes on 165 kPa (filled symbols) and 1.3 kPa (open symbols) poly-L-lysine-coated PAA gels. Each coloured line represents a different liposome sample. **d**, Spread area of liposomes on gels with modulus $E = 1.3$ kPa (same as **c**) over longer times. **e**, TR-DHPE at the contact zone immediately before rupture, at 65 s (green) and during rupture at 70 s (red). White dotted line indicates zoomed-in region below.

maximum contact area within the first 10–20 s (Fig. 1c). The similar spreading dynamics at early times indicate that the first phases of spreading (P1/P2) are unaffected by substrate stiffness and suggest a similar extent of excess membrane in the two conditions. After 10 s, the liposomes transition to a slower phase of spreading (P3) as indicated by a shallow slope of the curve of area versus time. On 165 kPa substrates, the liposomes terminate P3 and subsequently rupture with a mean time of 17±14 s ($N = 28$) from initial contact with the surface (Supplementary Movie 1). In contrast, the mean time to rupture for liposomes on soft gels is much longer, of 198±36 s ($N = 31$). Strikingly, in the P3 phase on soft gels, the liposome contact area decreases by 4.0±1.2% ($N = 13$) before rupture (Fig. 1d,e and Supplementary Movie 2), whereas it remains constant on hard gels. These data indicate that the nature of the P3 phase of spreading is qualitatively altered on sufficiently soft substrata.

Liposome adhesion induces a uniform, three-dimensional traction strain. By embedding 40 nm fluorescent beads within the PAA gel, the extent to which the underlying hydrogel is deformed during P3 can be observed (Fig. 2a,b). Using particle imaging velocimetry to calculate the x–y displacement, inward displacements of the PAA gel are observed and increase over time (Fig. 2c and Supplementary Movie 3). This indicates that the vesicle induces a contraction of the underlying PAA gel in the horizontal plane that increases with time.

Concomitant with the observed gel displacement in the x–y plane, we also observe a decrease in the fluorescence intensity of beads beneath the liposome in comparison with those far away from the liposome (Fig. 2b and Supplementary Fig. 2 and Movie 4). This indicates that the gel is also displaced in the z direction. We estimate the displacement in the z direction (u_z) immediately before rupture ($t = t_0$) by using a three-dimensional (3D) point-spread function to translate the decrease in fluorescence intensity of beads beneath the liposome into a displacement of the surface of the gel (Fig. 2d,e and Supplementary Fig. 2). This displacement is measured from the origin at the contact line to the centre of the liposome. The displacement reflects the total distance between the lowest point in the substrate at a distance r from the centre of the liposome, and the height of the substrate at the contact line. Thus, by this estimate, the magnitude of u_z is highest towards the centre of the liposome ($r = 0$), and, decays to zero at the periphery of the liposome ($r = r_0$). We also note that the magnitude of the in-plane displacement (dr) at the periphery of the liposome is roughly equivalent to the magnitude of the out-of-plane displacement (u_z) at the centre of the liposome (Fig. 2g). By conservation of gel volume, there is an upward displacement of the gel far from the liposome (Supplementary Movie 4).

The substrate deformation is quantified by a strain energy, which increases over time as the liposome contact area decreases (Fig. 2f).

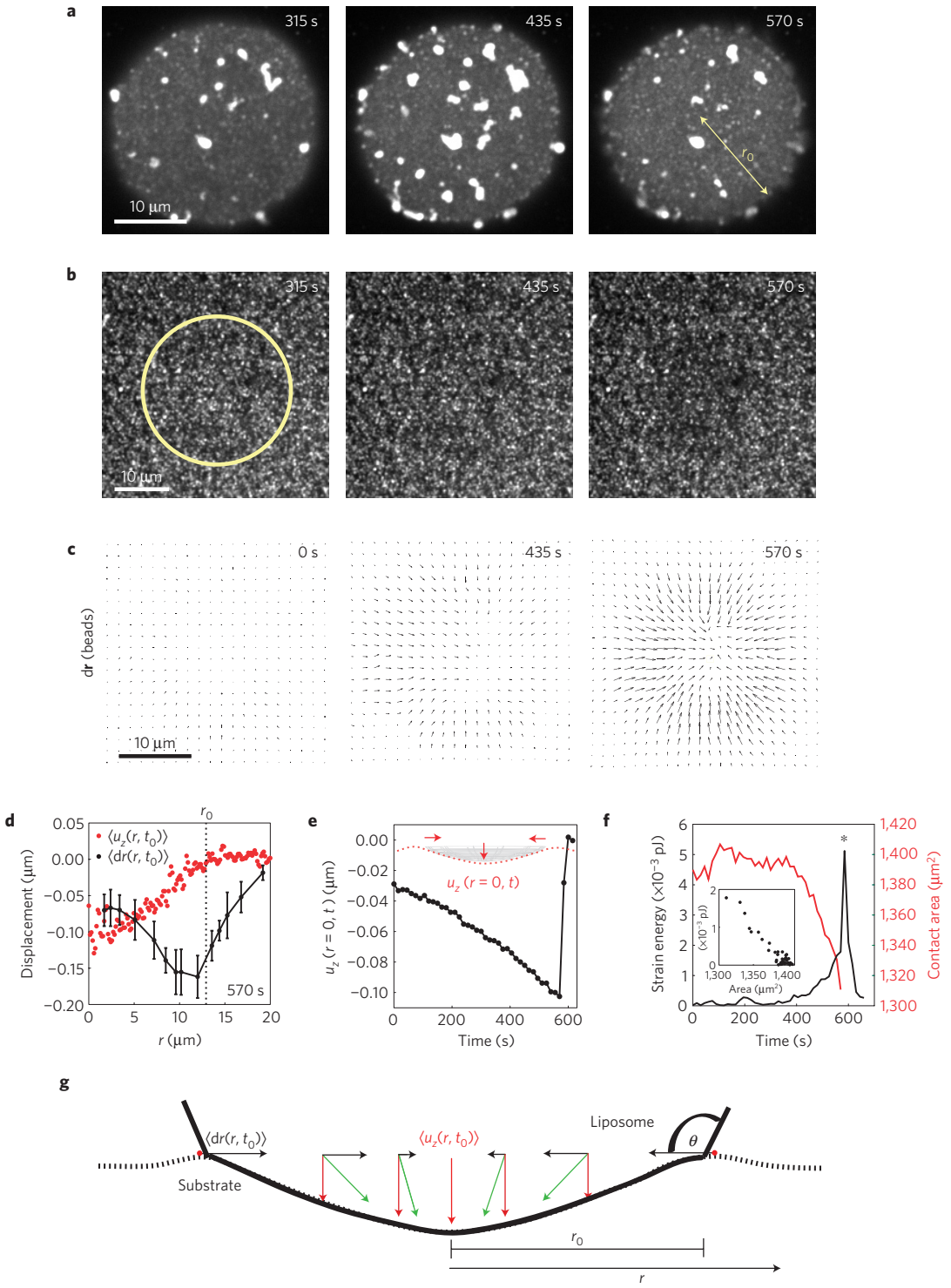

Figure 2 | Liposome adhesion deforms soft substrates. a, Fluorescence images (TR-DHPE) of a liposome during contraction on a 1.8 kPa gel, 315, 435 and 570 s after the start of P3. **b**, Fluorescence images of 40 nm beads beneath the liposome in **a**. The circle indicates the position of the liposome in **a**. **c**, Substrate deformation measured by displacement of embedded beads shown in **a** (×10 magnified). **d**, Averaged radial bead displacement (black) and averaged *z*-bead displacement (red) as a function of distance from the centre of the liposome, *r*. Error bars indicate the standard deviation. **e**, *z*-displacement (u_z) of the centre of the liposome over time. Inset: diagram of the volume of the liposome that lies below the initial surface (red dotted line). **f**, Elastic strain energy (black) and liposome contact area (red) over time corresponding to the deformations of the gel in **c**. Inset: elastic strain energy plotted against contact area. **g**, Schematic of the radial displacement (black) and the vertical displacement (red) with the net displacement vectors (green) of a liposome at its peak contracted state.

During times of substantial substrate deformation, the contact area decreases and the substrate strain energy increases (Fig. 2f, inset). Thus, there is a direct correlation between the reduction in the contact area of the liposome and the gel contraction and we confirm that no slip occurs between the substrate and the membrane (Supplementary Fig. 3).

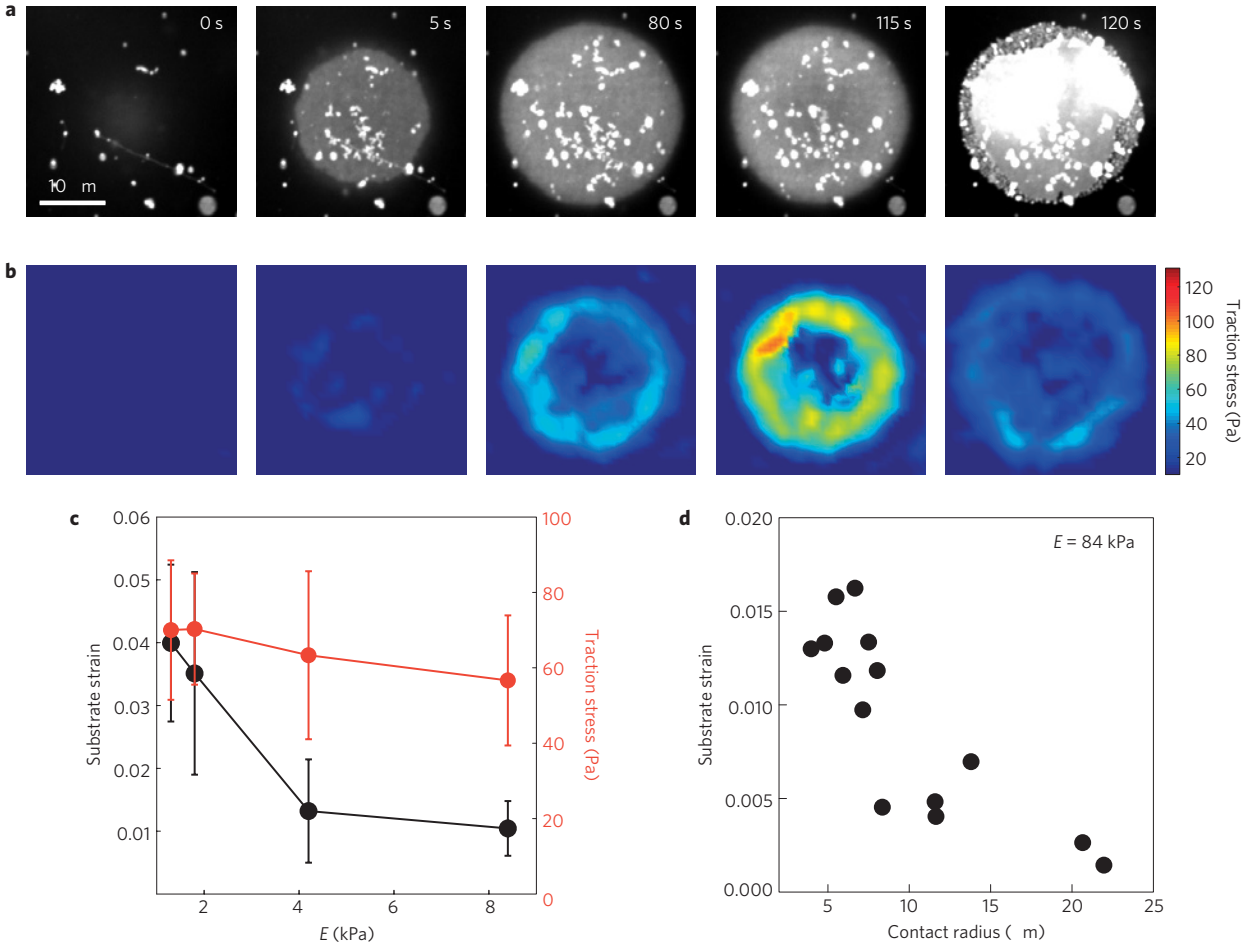

Figure 3 | Substrate traction stress varies with liposome size. a, Fluorescence images of a liposome spreading on a 1.3 kPa PAA gel at times after the start of P0. **b**, Calculated in-plane traction stress induced by the spreading of liposomes. **c**, Mean in-plane traction stress (red) and mean traction strain (black) for liposomes less than 17 μm in radius as a function of substrate stiffness, E. The traction stresses are measured for PAA stiffness, $E = 1.3$, 1.8, 4.2 and 8.4 kPa. Error bars indicate the standard deviation. The lines are intended to guide the eye. **d**, Mean in-plane traction strain as a function of the radius of the contact area between the liposome and substrate ($E = 8.4$ kPa).

We wondered whether the curving of the adhesion surface was simply generating this apparent decrease in projected area we observe, by an effect that would be purely geometric. We estimate the real area of the curved adhesion surface (Fig. 2e, inset), A_{3D}, by assuming it to be a truncated sphere with the observed depth u_z below the contact line. For a liposome at the peak in its strain immediately before rupture on a 1.8 kPa gel, we approximate that the 3D curved area differs from the 2D projected area by <0.01% (Supplementary Eqs 1,2). Thus, we consider the volume of the liposome to be essentially constant, as we do not observe large changes in the radius of the liposome that could account for the ∼3.5% strain we measure during contraction. Therefore, the 3D contact area undergoes a true negative strain in the reduction of the contact area.

Substrate traction stress is consistent with Laplace pressure. The indentation of the gel arises from the vertical force applied by the liposome to the elastic substrate. Mechanical equilibrium implies that a traction force located at the contact line balances the pressure P_i acting on the contact area between the substrate and the liposome. Writing the Laplace law at the free membrane of the liposome yields:

$$P_i - P_o = \frac{2\tau}{R_c}$$

where P_o is the pressure outside the liposome, and R_c is the radius of curvature of the upper side of the liposome, similar in magnitude to the radius of adhesion, r_0 (Supplementary Fig. 1). The lysis tension is approximately 0.3 mN m^{-1}, close to previous estimates[13,20]. By traction force microscopy[21], we show that tension builds within approximately 100 s (Fig. 3a,b), yielding a loading rate of ∼0.003 mN m^{-1} s^{-1}. At this loading rate, we expect a very weak dependence of lysis tension on rate and therefore consider it negligible[20,22]. At a tension of 0.3 mN m^{-1} close to the lysis tension, for a radius of 10 μm, and considering that $P_0 \ll P_i$, we find that P_i is approximately 60 Pa.

We assume here that the surface of the substrate is only weakly deformed and close to a planar surface (Supplementary Figs 1 and 2). The vertical force per unit length pulling the substrate upwards at the contact line is then $f = P_i r_0$, where r_0 is the radius of adhesion. We proceed here by analogy to the calculation of the deformation of a soft substrate by a sessile drop. In the vicinity of the contact line, the tensions dominate and the angles between the vesicle and the substrate are given by the classical Neumann triangle construction[23]. The competition between interfacial tensions and the shear modulus $\mu \approx E$ of the substrate define a length, $\ell \approx S/E$, where S is the spreading power of the vesicle on the substrate, which is of the order of the interfacial tension τ. This length is much smaller than the horizontal radius of the vesicle: $\ell/r_0 \approx 0.1$. Except in a boundary region of size ℓ in the vicinity of the contact

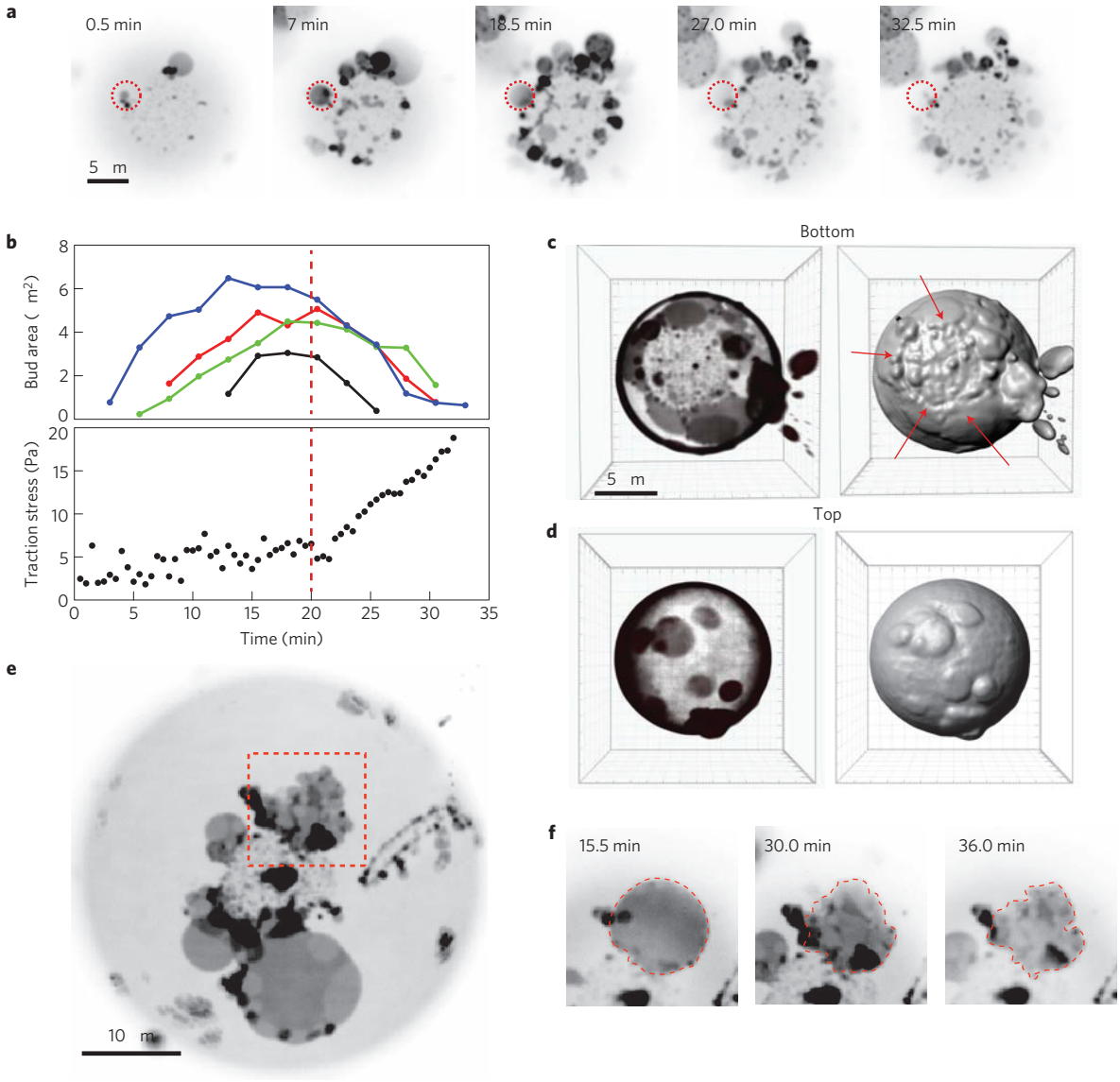

Figure 4 | Substrate contraction induces compression of the membrane and budding of the bilayer at the contact zone. a, 'Budding' of the membrane during the compression of the bilayer within the contact zone on a 1.8 kPa PAA gel during early P3 visualized by TR-DHPE fluorescence. The red line indicates the region over which the area is measured. **b**, Projected 2D area of the membrane buds in **a** over time, where each colour is a different bud (top); traction stress for the liposome over time (bottom). **c**,**d**, Confocal reconstruction of the bottom half (**c**) and top half (**d**) of an adherent liposome with 'budding' domains (TR-DHPE). Adjacent to each is the computed surface of the liposome showing a roughened surface. Red arrows point to membrane buds at the contact line. **e**, Image of a 3D projection of the bottom half of an adherent liposome showing buds emerging from the contact line. The red dotted line focuses on a bud that deflates in **f**. **f**, Bud deflates over time. Red line outlines bud. Images in **a**,**e**,**f** are inverted contrast.

line, the deformation of the substrate is dominated by elasticity and not by tension. We therefore calculate the deformation of the substrate due to the vertical force of the vesicle by considering only substrate elasticity. Assuming that the substrate is incompressible, we write that the stress at the surface balances the force exerted by the liposome, and obtain the vertical component u_z of the displacement of the surface in the centre of the adhesion area (see detailed calculation in Supplementary Information):

$$u_z(r=0) = -\frac{P_i r_0}{4\mu} = -\frac{3P_i r_0}{4E}$$

With P_i of the order of 60 Pa as estimated above, $E = 1.8$ kPa and an adhesion radius of the order of 10 μm, one finds a vertical displacement of 0.25 μm, which is in good agreement with our experimental measurement (Supplementary Fig. 2 and Movie 5). No deformation is observed ($u_z(r=0) = 0$) when pores are formed or when the liposome ruptures and $P_i = 0$ (Supplementary Fig. 4 and Movie 6).

Liposome contraction of the substrate induces compression of the bilayer within the contact zone. During late P3, the membrane adherent to the $E = 1.3$ kPa PAA gel undergoes a negative strain of up to ~4% (Fig. 3c) during adhesion and is therefore compressed. Bilayer compression has been shown to modulate the tubulation of membranes *in vitro*[24]. We also observe the formation of membrane defects that resemble outward projections during the P2–P3 stages of spreading (Fig. 4a). These projections we term 'buds'. Dynamically, buds may form at the contact line or within the contact area (Fig. 4a) and shrink as the liposome contracts the substrate (Fig. 4b). After formation at the contact surface, they may diffuse across the liposome surface (Fig. 4c,d)

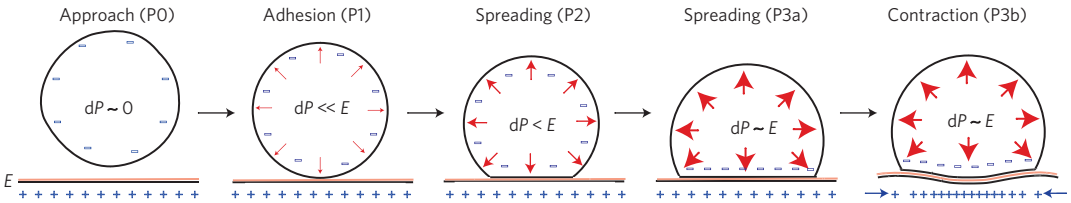

Figure 5 | Minimization of energy drives substrate contraction. Diagram of substrate contraction. The liposome minimizes its energy by deforming the substrate to increase the charge density (blue) at the cost of the elastic strain energy. The increased membrane tension due to adhesion elevates the Laplace pressure (red) and indents the substrate. The thickness of the arrows represents the magnitude of the hydrostatic pressure.

or rupture and deflate spontaneously (Fig. 4e,f). At 37 °C, the growth rate is comparable to 25 °C ($0.23 \pm 0.10\,\mu m^2\,min^{-1}$ versus $0.39 \pm 0.13\,\mu m^2\,min^{-1}$, Supplementary Fig. 5) although the rate of fusion is considerably higher (~30% versus ~6%, Supplementary Movie 7). Furthermore, the presence of buds is not reversed by osmotic shock (Supplementary Movie 8). Morphologically, buds are flat, 'pancake-like' structures, and are round at the contact line, but may be tubular within the contact area (Fig. 4c,d and Supplementary Movie 9). Buds are also enriched in fluorescent lipid (Supplementary Fig. 6) and are phase-separated (Supplementary Fig. 7) reminiscent of charge-induced domain formation in polyanionoic polymersomes[25].

Discussion

Our results show that the spreading of pure liposomes generates large traction stresses on compliant substrates. The measured traction stress is consistent with the stress generated by Laplace pressure. More interesting is the question of the mechanistic origin of these stresses. Note that deformations occur in the three dimensions: horizontally, we observe a radial contraction of the adhesion surface, and perpendicularly to the substrate is an indentation. Here, we present a simple model to propose that the horizontal, radial, contractile stresses are a result of adhesion on a deformable substrate whereas indentation is generated by an applied pressure through membrane tension elevated by adhesion to the substrate. When contact between the floppy, low-membrane-tension liposome and the substrate is initiated, spreading consists of smoothening out membrane undulation without significantly increasing membrane tension. Minimization of the total free energy is thus achieved by increasing the adhesion contact zone. Note that the adhesion energy E_a has, by convention, a negative sign and is taken to be proportional to the number of poly-L-Lysine-mediated bonds and therefore to the contact area by assuming negligible increase of poly-L-lysine–lipid interaction density at this stage. After exhaustion of excess membrane, an adhesion energy E_a^0 is reached, and further spreading occurs at the cost of elevated membrane tension because surface increases. The membrane tension consequently elevates the Laplace pressure, and generates a positive outward pressure difference reflected in the indentation of the substrate.

We speculate that the subsequent contraction of the substrate results from a minimization of the total energy $E_t = E_a + E_e$ of the system, where E_e is the elastic energy stored in the substrate. We assume here that the liposome volume is conserved and that the membrane is inextensible, so that the variation of the elastic energy stored in the membrane is neglected. In a first approximation the radius of adhesion, r_0, is hence assumed to be constant; the substrate is then undeformed so that $E_e^0 = 0$. The binding partners of poly-L-lysine are lipids; they can thus be recruited by diffusion and we assume that they are in excess in the contact area (Supplementary Fig. 6). The adhesion energy is therefore proportional to the number of poly-L-lysine molecules in the contact area and we write $E_a = -\alpha r_0^2 n_a$, where n_a is the surface density of poly-L-lysine of the substrate and α a positive constant that accounts for the adhesion strength. The key point is then that density depends on the change in contact area and follows $n_a \approx n_a^0(1-2\varepsilon)$, where $\varepsilon = dr/R$ is the strain of the substrate. In turn, contraction comes at the cost of the elastic energy stored in the substrate. This elastic energy E_e is proportional to the elastic modulus E, and depends quadratically on the strain, and therefore is proportional to ε^2. As r_0 is the characteristic length of the system, a dimensional analysis of the remaining terms gives $E_e \approx \beta E r_0^3 \varepsilon^2$, where E is the elastic modulus and β is a positive constant that accounts for the geometry of the system. These simple theoretical arguments then imply that the total energy E_e is minimized for a negative value of the strain $\varepsilon \approx -(\alpha n_a^0)/(\beta E r_0)$. This shows that contraction of the substrate can minimize the total energy and is therefore favourable, which, we suggest, is the mechanism responsible of our observations (Fig. 5). Moreover, as can be seen in Fig. 3d, we find that larger liposomes induce less traction strain than do smaller liposomes. This reduction in strain is consistent with the $1/r$ decrease of the above equation for the strain. Note that this model may be extended to incorporate potential 'solid-like' domains near the contact line, as was observed in similar charge-mediated membrane reorganization[25].

Liposome adhesion to rigid substrates has been shown to induce the formation of topological membrane defects such as blisters[12] and the separation of lipid species within the bilayer[26–28]. Separately, membrane projections have been observed in model lipid bilayers under compressive stress[24], reminiscent of the formation of 'blebs' that have been observed during cell spreading[29–31] and after osmotic shock[32]. Buds differ qualitatively from adhesion-induced blisters in liposomes and pressure-induced blebs in cells. First, the formation of buds follows the initial spreading of liposomes (P2–P3), and the buds disappear during contraction and tension increase whereas

Table 1 | Comparison of traction stresses of adherent cells on soft gels.

Cell	Mean stress (Pa)	Peak stress (Pa)	Gel stiffness (kPa)	Refs
Liposome	70	n/a	1.3	Current work
Human airway smooth muscle cells	32–90	450	1.3	35
Mouse embryonic fibroblasts	99	1,140	6.2	36
Bone osteosarcoma (U2OS)	96	300	2.8	37
Bovine aortic endothelial cells	200	400	1.0	38
NIH 3T3 fibroblasts	190	3,500	6.2	36

Mean stress is calculated as the average total force per cell, divided by the average cell area. The peak stress is the maximum stress measured at a focal adhesion. The gel stiffness is the elastic modulus of the gel at which the mean and peak stresses were measured.

blisters appear during spreading (P1) and remain. Second, buds may emerge at the periphery of the adhesion zone as opposed to purely within the adhesion zone itself and appear as flat, 'pancake-like' structures that are phase-separated, reminiscent of the charge-induced formation of domains polymersomes[25]. Thus, in our experiments we observe that buds are sensitive to both pressure and adhesion.

Hydrostatic forces are the restoring forces that balance tension generated on cellular length scales. To balance the tension, the liposome induces a vertical indentation of the gel, in line with previous observations of indentation of polymer cushions due to liposome adhesion[17] and the 3D deformation of adherent cells on substrates of physiologically relevant moduli[33,34]. However, through the use of substrates that are isotropically elastic, we report in plane radial stresses that accompany the vertical indentation that are comparable in magnitude to the mean traction stresses exerted by select cell types (Table 1). Thus, we show that liposomes can induce contraction mediated by adhesion, therefore transmitting mechanical stresses to their environment. Together, these results contribute to a more complete description of cell contractility, highlighting the important role of the membrane in generating stresses.

Received 28 June 2013; accepted 27 November 2013; published online 19 January 2014

References

1. Boucrot, E. & Kirchhausen, T. Endosomal recycling controls plasma membrane area during mitosis. *Proc. Natl Acad. Sci. USA* **104,** 7939–7944 (2007).
2. Raucher, D. & Sheetz, M. P. Membrane expansion increases endocytosis rate during mitosis. *J. Cell Biol.* **144,** 497–506 (1999).
3. Houk, A. R. *et al.* Membrane tension maintains cell polarity by confining signals to the leading edge during neutrophil migration. *Cell* **148,** 175–188 (2012).
4. Gauthier, N. C., Fardin, M. A., Roca-Cusachs, P. & Sheetz, M. P. Temporary increase in plasma membrane tension coordinates the activation of exocytosis and contraction during cell spreading. *Proc. Natl Acad. Sci. USA* **108,** 14467–14472 (2011).
5. Yeung, T. *et al.* Effects of substrate stiffness on cell morphology, cytoskeletal structure, and adhesion. *Cell Motil. Cytoskel.* **60,** 24–34 (2005).
6. Schwarz, U. S. & Gardel, M. L. United we stand: Integrating the actin cytoskeleton and cell-matrix adhesions in cellular mechanotransduction. *J. Cell Sci.* **125,** 3051–3060 (2012).
7. Batchelder, E. L. *et al.* Membrane tension regulates motility by controlling lamellipodium organization. *Proc. Natl Acad. Sci. USA* **108,** 11429–11434 (2011).
8. Lipowsky, R. & Seifert, U. Adhesion of membranes—a theoretical perspective. *Langmuir* **7,** 1867–1873 (1991).
9. Lipowsky, R. & Seifert, U. Adhesion of vesicles and membranes. *Mol. Cryst. Liq. Cryst.* **202,** 17–25 (1991).
10. Seifert, U. & Lipowsky, R. Adhesion of vesicles. *Phys. Rev. A* **42,** 4768–4771 (1990).
11. Albersdorfer, A., Feder, T. & Sackmann, E. Adhesion-induced domain formation by interplay of long-range repulsion and short-range attraction force: A model membrane study. *Biophys. J.* **73,** 245–257 (1997).
12. Nardi, J., Bruinsma, R. & Sackmann, E. Adhesion-induced reorganization of charged fluid membranes. *Phys. Rev. E* **58,** 6340–6354 (1998).
13. Murrell, M. *et al.* Spreading dynamics of biomimetic actin cortices. *Biophys. J.* **100,** 1400–1409 (2011).
14. Bernard, A. L., Guedeau-Boudeville, M. A., Jullien, L. & di Meglio, J. M. Strong adhesion of giant vesicles on surfaces: Dynamics and permeability. *Langmuir* **16,** 6809–6820 (2000).
15. Brochard-Wyart, F. & de Gennes, P. G. Adhesion induced by mobile binders: Dynamics. *Proc. Natl Acad. Sci. USA* **99,** 7854–7859 (2002).
16. Cuvelier, D. & Nassoy, P. Hidden dynamics of vesicle adhesion induced by specific stickers. *Phys. Rev. Lett.* **93,** 228101 (2004).
17. Limozin, L. & Sengupta, K. Modulation of vesicle adhesion and spreading kinetics by hyaluronan cushions. *Biophys. J.* **93,** 3300–3313 (2007).
18. Olbrich, K., Rawicz, W., Needham, D. & Evans, E. Water permeability and mechanical strength of polyunsaturated lipid bilayers. *Biophys. J.* **79,** 321–327 (2000).
19. Sandre, O., Moreaux, L. & Brochard-Wyart, F. Dynamics of transient pores in stretched vesicles. *Proc. Natl Acad. Sci. USA* **96,** 10591–10596 (1999).
20. Evans, E., Heinrich, V., Ludwig, F. & Rawicz, W. Dynamic tension spectroscopy and strength of biomembranes. *Biophys. J.* **85,** 2342–2350 (2003).
21. Sabass, B., Gardel, M. L., Waterman, C. M. & Schwarz, U. S. High resolution traction force microscopy based on experimental and computational advances. *Biophys. J.* **94,** 207–220 (2008).
22. Hategan, A., Law, R., Kahn, S. & Discher, D. E. Adhesively-tensed cell membranes: Lysis kinetics and atomic force microscopy probing. *Biophys. J.* **85,** 2746–2759 (2003).
23. Style, R. W. & Dufresne, E. R. Static wetting on deformable substrates, from liquids to soft solids. *Soft Matter* **8,** 7177–7184 (2012).
24. Staykova, M., Holmes, D. P., Read, C. & Stone, H. A. Mechanics of surface area regulation in cells examined with confined lipid membranes. *Proc. Natl Acad. Sci. USA* **108,** 9084–9088 (2011).
25. Christian, D. A. *et al.* Spotted vesicles, striped micelles and Janus assemblies induced by ligand binding. *Nature Mater.* **8,** 843–849 (2009).
26. Hategan, A., Sengupta, K., Kahn, S., Sackmann, E. & Discher, D.E. Topographical pattern dynamics in passive adhesion of cell membranes. *Biophys. J.* **87,** 3547–3560 (2004).
27. Gordon, V. D., Deserno, M., Andrew, C. M. J., Egelhaaf, S. U. & Poon, W. C. K. Adhesion promotes phase separation in mixed-lipid membranes. *Europhys. Lett.* **84,** 48003 (2008).
28. Rouhiparkouhi, T., Weikl, T. R., Discher, D. E. & Lipowsky, R. Adhesion-induced phase behavior of two-component membranes and vesicles. *Int. J. Mol. Sci.* **14,** 2203–2229 (2013).
29. Norman, L., Sengupta, K. & Aranda-Espinoza, H. Blebbing dynamics during endothelial cell spreading. *Eur. J. Cell Biol.* **90,** 37–48 (2011).
30. Norman, L. L., Brugues, J., Sengupta, K., Sens, P. & Aranda-Espinoza, H. Cell blebbing and membrane area homeostasis in spreading and retracting cells. *Biophys. J.* **99,** 1726–1733 (2010).
31. Myat, M. M., Anderson, S., Allen, L. A. & Aderem, A. MARCKS regulates membrane ruffling and cell spreading. *Curr. Biol.* **7,** 611–614 (1997).
32. Dai, J. W., Sheetz, M. P., Wan, X. D. & Morris, C. E. Membrane tension in swelling and shrinking molluscan neurons. *J. Neurosci.* **18,** 6681–6692 (1998).
33. Delanoe-Ayari, H., Rieu, J. P. & Sano, M. 4D traction force microscopy reveals asymmetric cortical forces in migrating *Dictyostelium* cells. *Phys. Rev. Lett.* **105,** 248103 (2010).
34. Maskarinec, S. A., Franck, C., Tirrell, D. A. & Ravichandran, G. Quantifying cellular traction forces in three dimensions. *Proc. Natl Acad. Sci. USA* **106,** 22108–22113 (2009).
35. Wang, N., Ostuni, E., Whitesides, G. M. & Ingber, D. E. Micropatterning tractional forces in living cells. *Cell Motil. Cytoskeleton* **52,** 97–106 (2002).
36. Yip, A. K. *et al.* Cellular response to substrate rigidity is governed by either stress or strain. *Biophys. J.* **104,** 19–29 (2013).
37. Oakes, P. W., Beckham, Y., Stricker, J. & Gardel, M. L. Tension is required but not sufficient for focal adhesion maturation without a stress fiber template. *J. Cell Biol.* **196,** 363–374 (2012).
38. Califano, J. P. & Reinhart-King, C. A. Substrate stiffness and cell area predict cellular traction stresses in single cells and cells in contact. *Cell. Mol. Bioeng.* **3,** 68–75 (2010).

Acknowledgements

We acknowledge financial support from NSF Grant DMR-0844115 for postdoctoral fellowship support to M.P.M. as well as the ICAM Branches Cost Sharing Fund. M.G. acknowledges support from the Burroughs Wellcome CASI award, Packard Foundation, and University of Chicago MRSEC. M.P.M. and C.S. acknowledge support from the French Agence Nationale de la Recherche (ANR) Grant ANR 12BSV5001401, and the Fondation pour la Recherche Médicale Grant DEQ20120323737. We thank U. Schwarz (University of Heidelberg) for use of traction force algorithms.

Author contributions

M.P.M. performed experiments. M.L.G. developed analytical tools. R.V., J-F.J., P.N. and C.S. contributed theory and calculations. M.P.M., R.V., J-F.J., P.N., C.S. and M.L.G. wrote the paper.

Additional information

Supplementary information is available in the online version of the paper. Reprints and permissions information is available online at www.nature.com/reprints. Correspondence and requests for materials should be addressed to M.P.M.

Competing financial interests

The authors declare no competing financial interests.